Bull. Mater. Sci., Vol. 39, No. 1, February 2016, pp. 167–175. © Indian Academy of Sciences.

Processing and characterization of extruded PET and its r-PET and MWCNT nanocomposite thin films by spin coating

ARVIND R SINGH[1,2] and VINEETA D DESHPANDE[1,*]

[1]Department of Physics, Institute of Chemical Technology, Matunga, Mumbai 400 019, India
[2]Department of Physics, G.N. Khalsa College, University of Mumbai, Mumbai 400 019, India

MS received 12 May 2015; accepted 17 August 2015

Abstract. **The objective of the present study was basic understanding of the formation of thin film morphology by spin coating using reorganized polyethylene terephthalate (r-PET) and multiwalled carbon nanotubes (MWCNTs) as fillers in PET. A study of the correlation between physical properties of the PET films and its surface morphology was carried out using atomic force microscopy-based power spectral density (PSD) analysis. No significant work of surface analysis, using PSD of thin films of PET has been reported till date. Dilute solution of PET, PET with 3 wt% (r-PET) and PET with 3 wt% (2 wt% r-PET + 1 wt% MWCNT) filler were prepared using trifluoroacetic acid (TFA) as a solvent and thin films were fabricated on glass substrate by the optimized spin coating technique. Preparation of r-PET and r-PET+ MWCNT fillers was obtained by the precipitation method using TFA as a solvent and acetone as an antisolvent. The samples before spin coating were extruded and for comparison, a film of non-extruded PET was also prepared. Structural studies by Fourier transform infrared and X-ray diffraction show higher degree of crystallinity in r-PET and decrease in chain entanglements. Owing to the crystallizing behaviour of r-PET, it allows better dispersion of MWCNT in the polymer matrix as compared with PET. The samples with fillers of MWCNT show more compact and unique mesh-like globular structure, indicating application for electromagnetic shielding foams and fibres.**

Keywords. **Thin films; precipitation; MWCNT; nanocomposite; AFM; PSD.**

1. Introduction

Since the discovery of carbon nanotube (CNT) by Lijima [1], it is extensively used as filler in polymers to prepare polymer nanocomposites. This is basically because of its high mechanical strength, high thermal and electrical conductivity, and good chemical stability [2,3]. Polymer composite prepared using CNT leads to better material properties such as mechanical strength, electrical conductivity, fracture toughness, electromagnetic shielding properties, etc. Polyethylene terephthalate (PET) is a semicrystalline polymer with excellent thermal stability, good mechanical properties, high chemical resistance, and low gas permeability [4]. Conductivity of PET increases with the addition of CNT signifying its use for flexible solar substrate. A number of papers have reported change in conformational and structural variations in extruded PET as compared with non-extruded PET [5]. Studies have shown variation in trans and gauche conformers after heat treatment which leads to considerable change in final product [6–8]. Heating of PET during extrusion process makes PET chains more ordered which is because of conformational change of PET chains. This variation drastically effects the incorporation of fillers in PET matrix. For studying polymer–filler matrix which is processed by solvent-induced methods such as solution casting, spin coating, or solvent electrospinning, there is need to properly incorporate effect of extrusion.

Precipitation method also called as coagulation method to prepare nanocomposites of multiwalled carbon nanotubes (MWCNTs) and PET was first used by Hu *et al* [9]. MWCNT/PET nanocomposite was prepared using ODCB–phenol (1 : 1 by mass) as a solvent and methanol as an antisolvent. Wrapping and better dispersion of MWCNT was reported by Hsiao *et al* [10] for preparing MWCNT/polyethylene. Although there is tremendous importance for precipitation method, very less literature is available on dispersing of MWCNT and preparing polymer nanocomposites which leads to better thermal, mechanical, and decreased electrical and rheological threshold [11]. Dispersion of nanofiller is a big challenge and the precipitation method can play a very important role by producing polymer wrapped MWCNT which can in fact used as filler for preparing polymer nanocomposites.

The structural and surface morphology of the materials play crucial role for their use in practical thin film devices. Thin films prepared by the spin coating technique is one of the best techniques to prepare organic film owing to its efficiency and reproducibility [12]. The films prepared by spin coating are influenced by factors such as concentration of the film-forming materials, molecular weight and solvent type (viscosity, density and surface energy), spinning rate, and operation temperature [13,14]. By controlling these

*Author for correspondence (vd.deshpande@ictmumbai.edu.in)

parameters desired and optimum results in terms of roughness and thickness can be achieved. A study of the correlation between physical properties of the PET films and its surface morphology is necessary for more comprehensive understanding for the improvement of the quality of these films for the technological applications. No significant work of surface analysis, using power spectral density (PSD) of thin films of PET has been reported. In the present work, the structural and morphology properties of prepared films were investigated. Surface imaging as well as statistical analysis, was used to characterize the local and overall roughness, grain size with the help of the PSD technique.

The spin coating parameters such as rpm, time for film forming, and acceleration time were first optimized in terms of the resulting film morphology. Spin coating of thin films prepared are helpful to study the structural and morphological phenomena relevant to fibre and textile processing at the molecular level. Structural properties of the films were investigated by Fourier transform infrared spectroscopy (FTIR) and X-ray diffraction (XRD). Morphological studies were carried out by scanning electron microscopy (SEM), atomic force microscopy (AFM) and polarizing optical microscopy (POM). The values of PSD for the AFM digital data were determined by the fast Fourier transform (FFT) algorithms instead of the root-mean-square (RMS) and peak-to-valley values. The PSD plots of prepared films are successfully approximated by the *ABC* model. Thin film samples of PET, PET with 3 wt% (r-PET), and PET with 3 wt% (2 wt% r-PET + 1 wt% MWCNT) were prepared by spin coating on glass substrate using trifluoroacetic acid (TFA) as a solvent. Preparation of r-PET and r-PET+MWCNT fillers was obtained by the precipitation method using TFA as a solvent and acetone as an antisolvent. The samples before spin coating were extruded and for comparison, a film of non-extruded PET was also prepared. The optimization was carried out by preparing the thin films at different rpm, concentration of solvent and spinning time. After morphological study of films with different rpm, further samples were prepared on the best spin coating parameter.

2. Materials

PET with melting temperature of 265°C and molecular weight ca. 20,000–30,000 was provided by the PET division of Reliance Industries (Patalganga, India). MWCNTs of 98% purity with average length of 10–30 μm and average diameter 20–30 nm were purchased from Nanoshell LLC, USA. TFA with boiling temperature of 72.4°C was obtained from S.D. Fine Chemicals (Mumbai, India).

3. Experimental

3.1 *Preparation of r-PET and r-PET with MWCNT*

PET was structurally modified by a precipitation technique [15,16]. Briefly, 6% by (w/v) of PET was dissolved in TFA and heated to 50°C with rapid stirring to completely dissolve the polymer. The heated polymer solution was precipitated by gradually adding the solution dropwise to 300 ml of acetone which was kept for stirring at room temperature. A white precipitate was obtained and it was washed with acetone and dried in a vacuum oven overnight at 40°C to obtain dry r-PET.

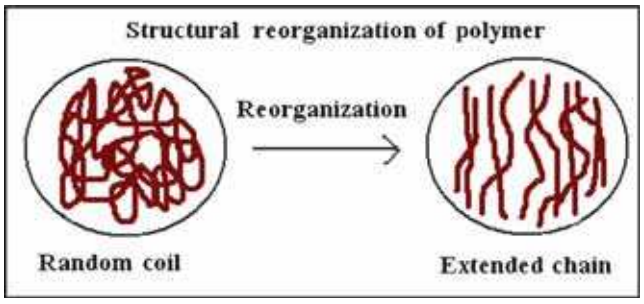

Figure 1. Schematic representation of the preparation of reorganized PET.

For preparing r-PET with MWCNT composite, MWCNT are first dispersed in TFA by energetic agitation using probe sonicator at a frequency of 20 kHz for 30 min. Briefly, 5% by (w/v) of PET was dissolved in TFA at 50°C associated by magnetic stirring. As soon as PET got dissolved in TFA, the dispersed solution of MWCNT in TFA was added to PET–TFA solution maintaining the total solution of PET/TFA as 6% by (w/v). The obtained solution was precipitated and was then washed and dried with the above method used for r-PET (figure 1).

3.2 *Extrusion of samples*

The samples of PET, PET with 3 wt% (r-PET), and PET with 3 wt% (2 wt% r-PET + 1 wt% MWCNT) were extruded using a counter rotating twin-screw extruder (Haake Rheocord 9000, TW100). The screw speed was maintained at 40 rpm and the temperature profiles for blending were 200°C for zone 1, 220°C for zone 2, 265°C for zone 3 and 270°C for the die zone. The extrudated samples were quenched in water at room temperature and palletized. The quenched samples were then reheated at 75°C for 4 h to remove any trapped moisture.

3.3 *Spin coating of the samples*

Thin film samples of PET, PET with 3 wt% (r-PET), and PET with 3 wt% (2 wt% r-PET + 1 wt% MWCNT) fillers were prepared by spin coating on glass substrate using TFA as a solvent at 3000 rpm for 90 s. For comparison with extruded sample of PET, non-extruded PET thin film sample was also prepared by above-mentioned spin coating parameters. Optimization of spinning rate was performed by preparing samples of non-extruded PET with different rpm of 1000, 3000, 5000 and 8000. The thickness of the deposited film was

determined with the help of sensitive microbalance using the relation

$$t = m/\rho A, \tag{1}$$

where m is the mass of the deposited film, A the area of the deposited film and ρ the density of the deposited material (PET = 1.38 g cm^{-3} [17,18]. Weight of the glass substrate with and without the deposited film was measured. The film thickness of the prepared samples by spin coating was found to be 30 μm. The nanocomposite films of non-extruded PET, extruded PET, PET with 3 wt% (r-PET), and PET with 3 wt% (2 wt% r-PET + 1 wt% MWCNT) are designated with PET A, PET B, PET C and PET D, respectively.

4. Characterization

4.1 *FTIR*

The spectra of samples were recorded in attenuated total reflection (ATR) mode by Perkin Elmer model Spectrum 100 FTIR. The range of spectra was 4000–400 cm^{-1} with a scan rate of 4 cm^{-1}.

4.2 *XRD*

The diffraction patterns for the films were recorded at ambient conditions on a Rigaku Instruments (Geldermalsen, The Netherlands, model Rigaku Miniflex II) with Cu Kα irradiation source. The data was recorded in continuous scan mode at a scan speed of 3 deg min^{-1}. The supply voltage and current were set to 30 kV and 15 mA, respectively.

4.3 *SEM*

Surface morphology of the films was investigated using FEI Quanta-200 model SEM with an operating voltage of 15 kV.

4.4 *AFM*

AFM measurements were performed with diInnova from Veeco Instruments. All AFM measurements were performed in tapping mode (for both trace and retrace information) using a silicon nitride tip at ambient temperature and the quantitative analysis was carried out using Veeco SPM Lab Analysis software.

4.5 *POM*

The films were examined at a magnification of 40× with Olympus, BX 53 POM. The microscope used was fitted with charge coupling device (CCD) camera interfaced with computer.

5. Results and discussion

5.1 *FTIR spectroscopy*

Figure 2 shows FTIR spectra in the range of 1400–800 cm^{-1}. The CH_2 wagging band observed at 1340 cm^{-1} has been associated with trans conformations of the ethylene glycol unit and the CH_2 wagging mode band at about 1370 cm^{-1} is assigned to the gauche conformation. Also, the CH_2–O stretching vibration at band 971 cm^{-1} has been associated with ethylene glycol units in the trans conformation. The intensity of 971 and 1340 cm^{-1} infrared absorption increases which clearly indicates that the population of the trans conformations increases for PET C and PET D as compared with PET A and PET B samples [16,19]. This suggests more extended and opened up chains for PET C and PET D.

The component of the ring bending mode at 1021 cm^{-1} denotes the position of benzene ring vibrations which has been associated with a more ordered environment of PET chains. There is increase in peak intensity at 1021 cm^{-1} for PET C and PET D. Comparing the peak intensity for trans and gauche conformations, it can also be seen that PET B shows more resolved peaks for trans conformation as compared to PET A. This shows extruded and its nanocomposites have higher degree of chain orientation and increase in trans conformation. These conformational variations are due to the influence of inter-chain interactions; which leads to changes in local and longer range conformational structure of the chain due to intra-chain interactions [20–22].

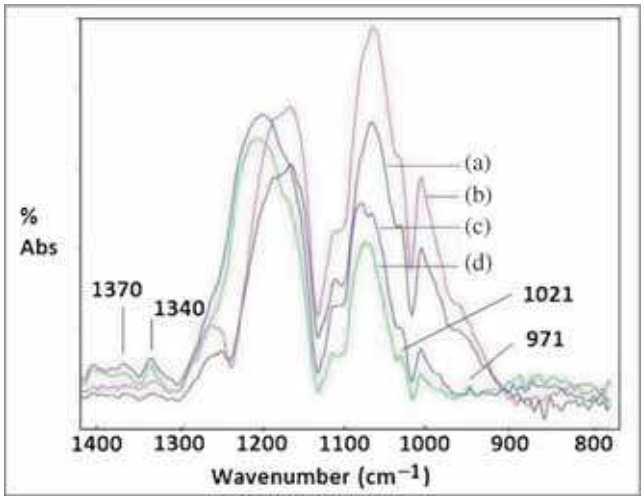

Figure 2. FTIR spectra of (**a**) PET A, (**b**) PET B, (**c**) PET C and (**d**) PET D.

Table 1. Variation of FWHM, 2θ, crystallite size and strain determined from XRD data.

Samples	FWHM (deg)	2θ (deg)	D (Å)	Strain (deg)	Crystallinity (%)
PET A	13.28	25.64	6.18	3.21	21.16
PET B	13.54	25.75	6.15	3.22	24.30
PET C	14.08	25.93	6.12	3.24	26.78
PET D	14.55	26.04	6.07	3.27	31.78

5.2 *XRD*

Diffraction peaks observed at $2\theta = 17.1°$, 22.6°, and 26° are assigned to (010), $(1\bar{1}0)$ and (100) lattice planes [20–22]. The full-width at half-maximum (FWHM), crystallite size, 2θ, and strain were calculated (table 1). The crystallite size was determined using the Scherrer formula. The FWHM was found to increase and crystallite size decrease for extruded sample as compared with non-extruded sample of PET. Similar decrease in crystallite size is also seen for nanocomposite samples prepared using of r-PET and MWCNT as fillers. The decrease in crystallite size and increase in strain of samples with fillers is due to the fact that more nucleation sites are produced during the formation of solid phase of the composite during film preparation. This behaviour of PET C and PET D is due to extended and oriented chains of r-PET.

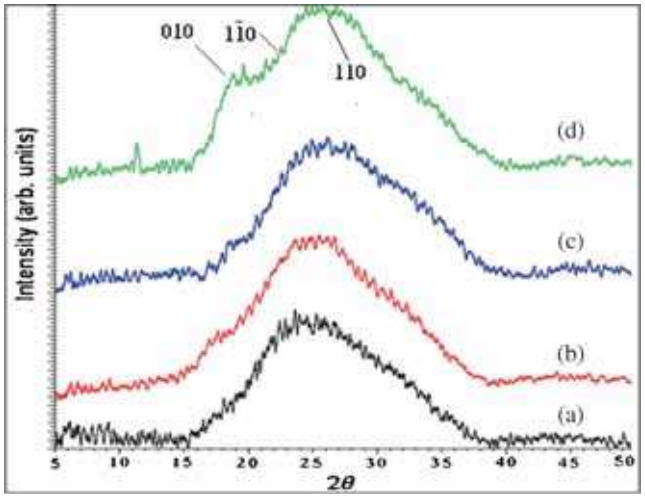

Figure 3. XRD spectra of (**a**) PET A, (**b**) PET B, (**c**) PET C and (**d**) PET D.

There is increase in peak intensity and peaks were shifted towards higher 2θ values from PET A to PET D. The peak intensity in diffractogram at 26.04° represents for samples with higher level of crystalline orientation [19]. Since crystallinity depends upon the periodicity, i.e., long-range order polymer molecules, periodicity is more with high intensity of lattice planes. PET C and PET D generally are showing higher level of crystalline orientation as compared with PET A and PET B. The diffractogram of PET D shows that relative increase in the peak intensities is largest for a peak at 26.2°; peak intensities for other two peaks for the same composite also show increase. The increase in peak intensities of r-PET over PET samples shows higher level of crystalline orientation in r-PET due to decrease in chain

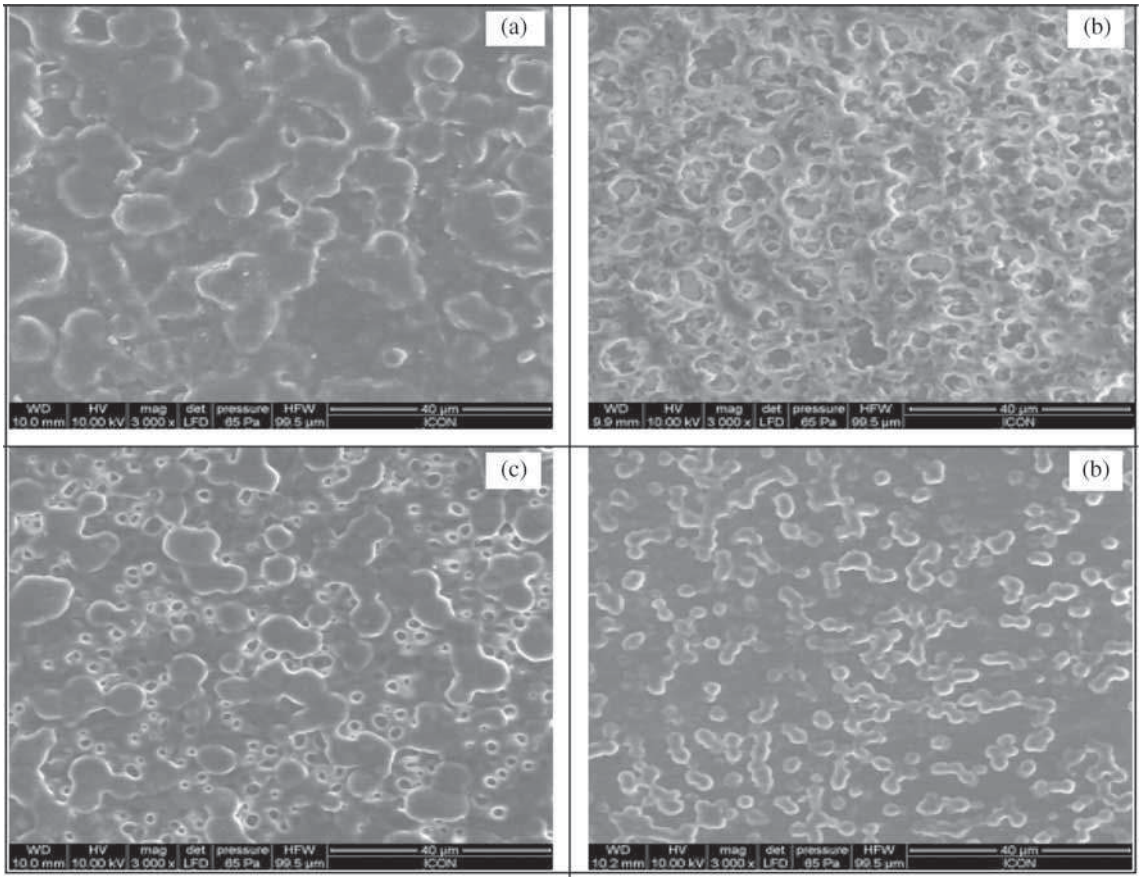

Figure 4. SEM image of PET non-extruded films prepared at (**a**) 1000, (**b**) 3000, (**c**) 5000 and (**d**) 8000 rpm.

entanglements. Quantitative determination of degree of crystallinity was carried out by using the formula

$$Q = I_c/(I_c + I_a), \tag{2}$$

where I_c is the intensity of diffracted beam from crystalline part and I_a the intensity of diffracted beam from amorphous part.

As seen from table 1, percentage crystallinity of extruded PET B is slightly higher as compared with unextruded PET A. PET C and PET D also show increase in % crystallinity. It can be seen that PET C sample shows higher degree of crystallinity as compared with PET A and PET B sample. PET D sample shows highest degree of crystallinity as compared with the other prepared samples. This increase in crystalline conforms are due to use of MWCNT as filler. As the chain entanglement decreases because of reorganization, MWCNT gets properly dispersed and creates more sites for crystallization which results into higher crystallization [23]. Similar confirmation of higher level of orientation in PET C and PET D as compared with PET A and PET B has also been reported in our FTIR results (figure 3).

5.3 *SEM*

Surface morphology of non-extruded PET films at rpm of 1000, 3000, 5000 and 8000 are shown in figure 4. Depending on rpm, thickness varies and accordingly morphology and roughness of the prepared samples are influenced. It can be seen that by varying spinning rate; which changes the thickness, the surface morphology changes which are evident from SEM images. The sample prepared at 3000 rpm shows compact and uniform structural morphology as compared with films prepared at other rpm. The surface morphology of films prepared at 1000 rpm shows balloon-type globular structure which converts into mesh-type globular structure at 3000 rpm. This could be due to increase in centrifugal force which breaks the big balloon-type structure and converts it mesh-type structure as rpm increases. But further increase in rpm to 5000 and 8000 changes the surface morphology to less compact and nonuniform morphology. This shows films prepared at 3000 rpm have compact and uniform structure which are ideal for preparing porous and mesh-type morphology which infact can be used for preparing electromagnetic shielding foams.

SEM image in figure 5 reveals formation of disc-type structure of PET A and PET B, whereas for PET C and PET D the surface morphology shows globular-type structure. The disc width is more for PET A as compared with PET B. The morphological studies reveal more compact and smooth surface of PET C and PET D nanocomposites as compared with PET A and PET B. This improved surface morphology of PET C and PET D could be due to decrease in chain entanglement density of r-PET [11,24]. The surface PET D

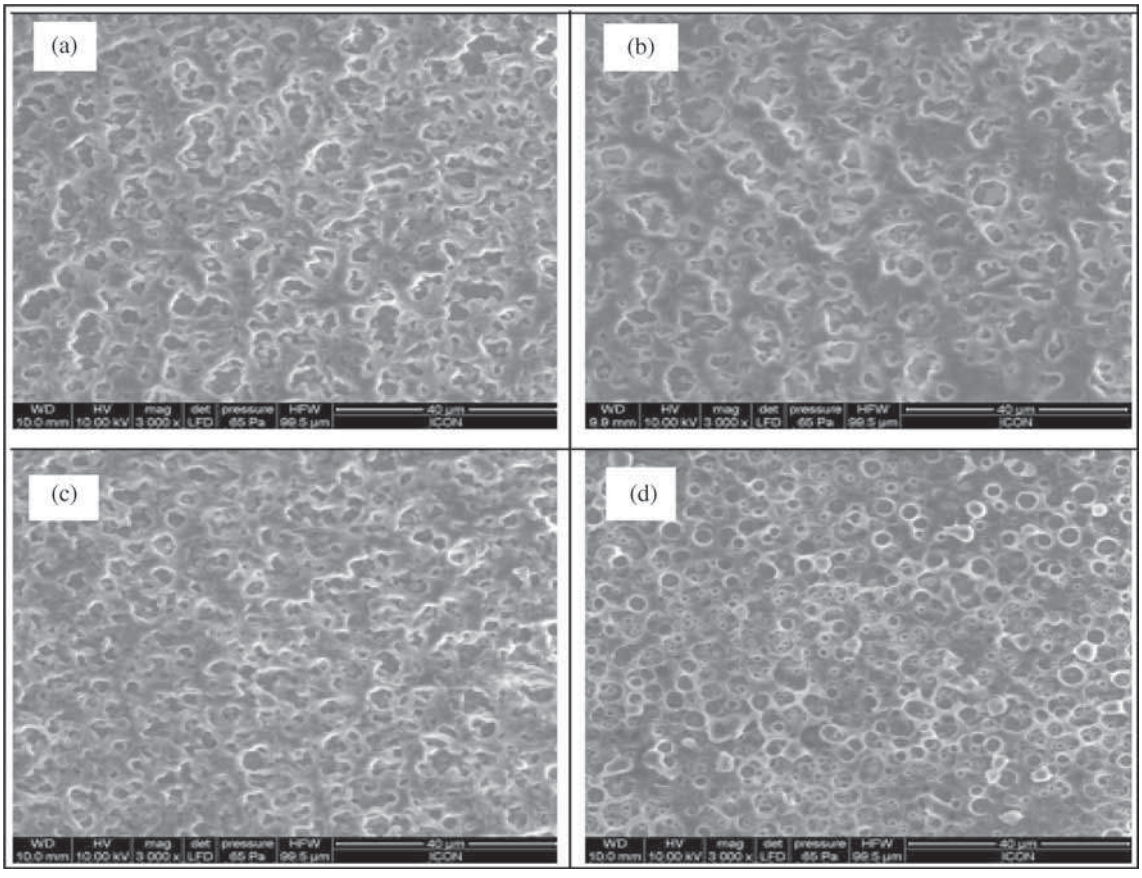

Figure 5. SEM image of films of (**a**) PET A, (**b**) PET B, (**c**) PET C and (**d**) PET D.

samples show more compact and uniform globular structure as compared with PET C. This could be due to more nucleation sites produced by MWCNT which leads to small and more uniform structure [16,19].

5.4 *AFM*

5.4a *Surface morphology by AFM height image*: Film of PET D shows a much higher concentration of small grains that are evenly distributed as compared with other prepared samples. The RMS roughness of PET A is 0.260 μm and it decreases for PET B and its nanocomposites. As seen from table 2, average height distribution of PET C and PET D samples decreases as compared with PET A and PET B which is due to extended chains of r-PET. PET D sample prepared using MWCNT along with r-PET as filler shows globular-mesh-type porous structure and compact morphology representing smoother surface as seen in figure 6. It can be suggested that due to extended and oriented chains of r-PET, MWCNT gets encapsulated by polymer and forms polymer wrapped MWCNT which acts as nucleating site for composite [9,25]. The average height (table 1) thus shows similar variation as RMS roughness in case of all samples.

Table 2. Variation of R_a, RMS and average height obtained from AFM with fluence.

Samples	Average surface roughness, R_a (μm)	RMS surface roughness (μm)	Average height (μm)
PET A	0.207	0.260	0.906
PET B	0.188	0.240	0.908
PET C	0.132	0.166	0.688
PET D	0.165	0.206	0.777

5.4b *PSD analysis*: The surface RMS roughness will be insufficient to supply the complete information of the surface modifications and PSD is evaluated to provide quantitative information about the surface roughness both in the vertical and lateral directions. The PSD curves of prepared films with *ABC* model fitting is shown in figure 7. Within the frame work of the *k*-correlation or *ABC* model, the auto-covariance function PSD_{ABC} for spatial frequency *f*,

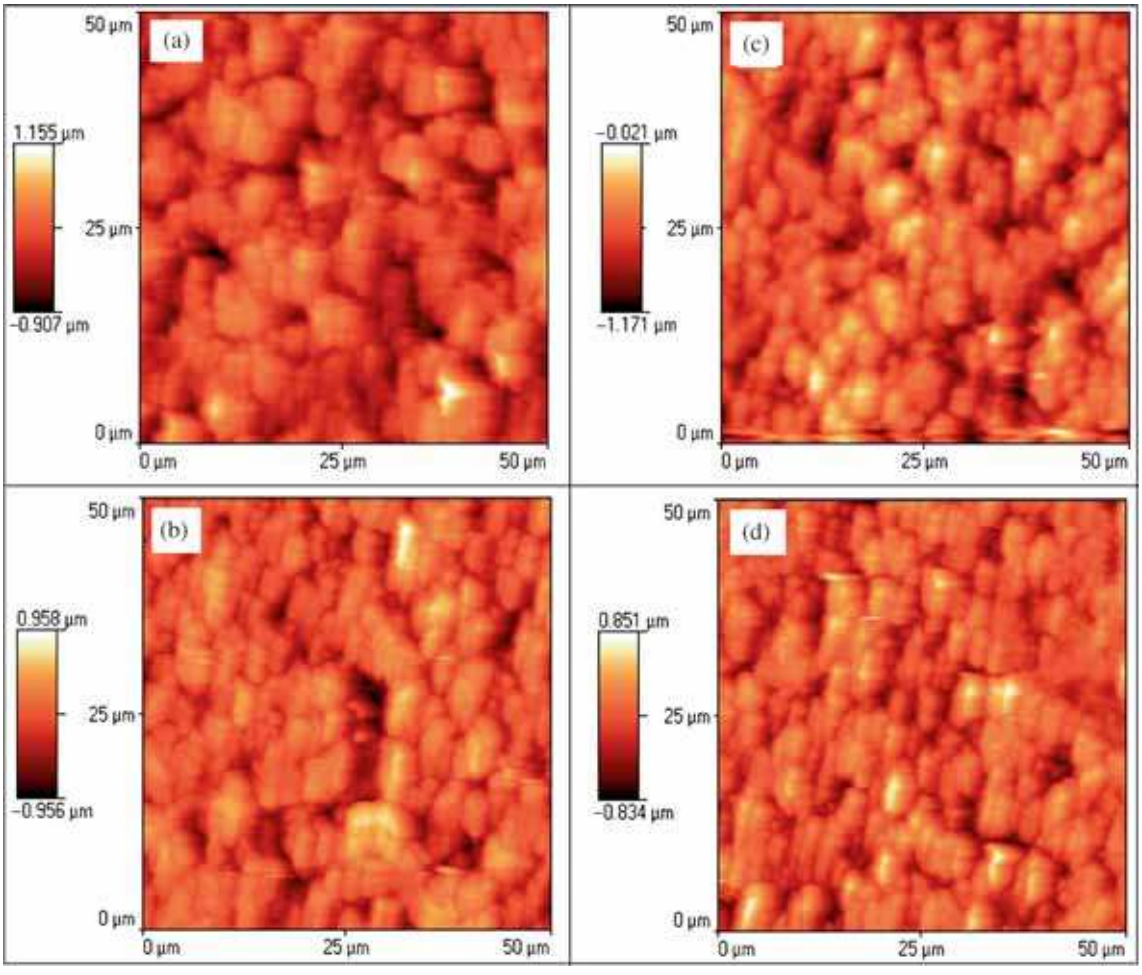

Figure 6. AFM images of (**a**) PET A, (**b**) PET B, (**c**) PET C and (**d**) PET D.

for a two-dimensional isotropically rough, self-affine fractal surface with a crossover region is given by

$$\mathrm{PSD}_{ABC} = (A)/\left(1 + B^2 f^2\right)^{(C+1)/2}, \quad (3)$$

where A, B and C are the function parameters [26,27].

At small f values, well below the 'knee' or the crossover region, the PSD is determined by A, which is related to the height of the surface roughness. For high values of f, beyond the 'crossover region', the PSD function is determined by C and tells us about fractalness of the surface. PSD plot is fitted in this *ABC* model and the values of A, B, C are given in table 3. The parameter A is higher for the PET A and PET C as compared with film of PET B and PET D which corresponds to peak-to-valley values. Grain size decreases significantly for the films of PET A to PET D. In mid-frequency range, the crossover point (knee) of PSD plot corresponding to X-axis gives correlation length which is related to mean grain size. The quantity B determines the position of the 'knee', which is related to the correlation length. The grain size for the films is given in table 3.

Although the surface morphology of PET D sample shows more compact and globular form representing smoother surface, but the roughness parameters shown in tables 2 and 3 show slight increase as compared with PET C samples. This increase in surface roughness and height structure could be due to formation of porous and mesh-type structure. The above results are in collaboration with SEM images.

The value of parameter C corresponds to the inverse slope of the PSD curve. It is reported that the film growth corresponding to the viscous flow, evaporation, and condensation, bulk diffusion and surface diffusion shows the value of C as 1, 2, 3 and 4, respectively. The value of C goes on decreasing for films from PET A to PET D. The value of C for samples of PET A and PET B are in the range of 3–4, whereas for PET C and PET D it is in the range of 4–5. The value of parameter C is highest for sample of PET D which shows there are more surface diffusion and variation [28]. This could be due to the increase in nucleation sites and smaller grain morphology due to r-PET and MWCNT in PET matrix. This improved composite provides more nuclei for crystallization and the number of spherulites also increases and hence the r-PET and its composites shows smooth and compact morphology which have also been shown by SEM images. As crystallization is related to and dependent upon microstructural properties, we can conclude from the above images that r-PET and its nanocomposites have all together

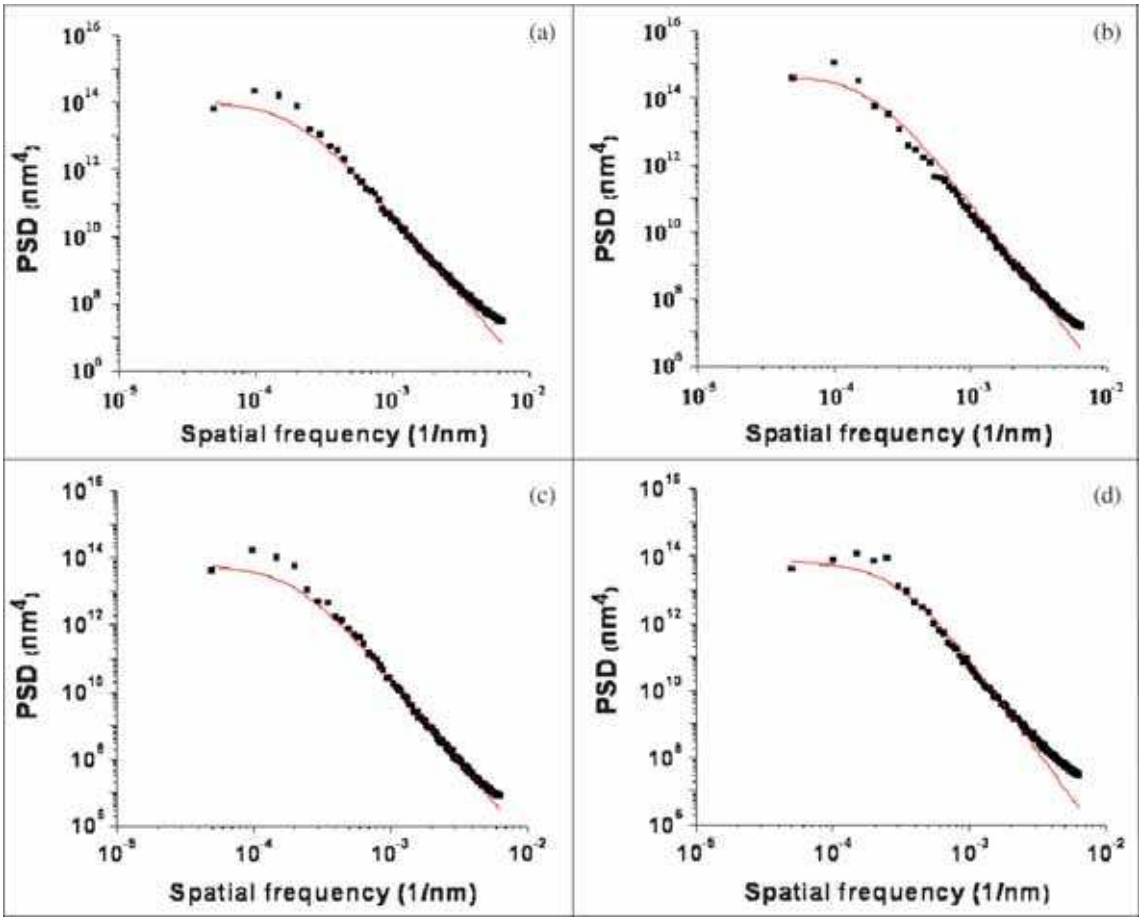

Figure 7. Power spectral density *vs.* spatial frequency plot of films fitted with *ABC* model of (**a**) PET A, (**b**) PET B, (**c**) PET C and (d) PET D.

Table 3. Parameters for k correlation model for PSD plots.

Samples	*ABC* model		
	A (nm^4)	B (nm)	C
PET A	1.08×10^{14}	5057	3.79
PET B	5.04×10^{14}	4786	3.93
PET C	6.19×10^{13}	4213	4.39
PET D	7.10×10^{13}	3251	4.60

different morphology and crystallizes in a manner different from PET.

5.5 *POM*

Figure 8 shows POM images of the prepared samples. Large spherulites have form for non-extruded PET A sample and smaller spherulites have formed for films prepared with extruded samples. This suggests PET B is crystallized from a very large number of nuclei due to extrusion. POM images of PET C sample smaller shows smaller spherulites in comparison with PET A and PET B samples. The reorganization of polymer leads to unentangled chains of r-PET. The film of PET C shows formation of small spherulites which are due to use of r-PET as filler which provides more nucleating sites. However it can be seen that PET D sample shows more compact and regular spatial distribution of spherulites as compared with other samples which suggests homogeneous nucleation of MWCNTs in polymer chains [29].

The crystallite size calculated from XRD of samples PET C and PET D prepared using r-PET and r-PET+MWCNT as filler decreased as compared with PET A and PET B. This decrease in crystallite size is a direct consequence of an increase in dispersion, which suggests uniform nucleation of fillers in polymer chains. Hence the films of PET C and PET D are crystallized from a very large number of nuclei and produced extremely small spherulites which also lead to decrease in surface roughness as seen from AFM analysis. Based on these observed POM images, it can be seen that the nucleation density and nucleation rates of samples prepared using r-PET and r-PET+MWCNT as filler are higher than other samples, which is consistent with other surface and structural data.

6. Conclusion

The results in present work revealed that use of r-PET and MWCNT as fillers in PET matrix provides better dispersion of MWCNT due to decrease in entanglement density and can effectively influence the crystallization development and surface morphology of the nanocomposites. The result also shows variation of properties of pristine polymer matrix due to extrusion. Crystalline structure studies with FTIR and XRD represent oriented samples which are crystallized with a higher level of crystalline orientation and increase in percentage crystallinity for samples prepared using r-PET and MWCNT as filler. The above results can be correlated with our surface morphological studies by SEM, AFM, and POM. The AFM surface imaging with PSD analysis has been used to analyse the mechanism of formation of film using spin coating. It can be suggested that due to extended chains of r-PET, MWCNT gets encapsulated by polymer and forms polymer wrapped MWCNT. This improved composite provides more nuclei for crystallization and the number of spherulites also increases and hence the r-PET and its composites shows smooth and compact morphology which have also been shown by SEM images. The reorganization of polymer and incorporation of conductive fillers will hence decrease electrical percolation threshold even with lower filler loadings. These properties will in fact allow preparing electromagnetic shielding foams and fibres.

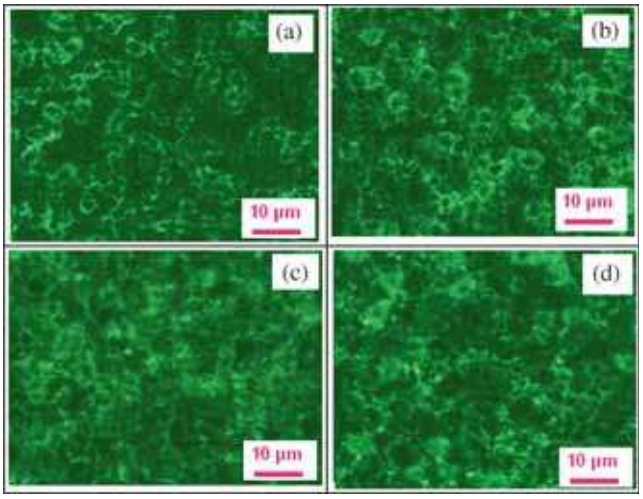

Figure 8. POM images of (**a**) PET A, (**b**) PET B, (**c**) PET C, and (**d**) PET D.

Acknowledgements

We are thankful to UGC for providing UGC-SAP Fellowship and UGC major Research project (F No. 41-881/2012 (SR)).

References

[1] Lijima S 1991 *Nature* **354** 56
[2] Moniruzzaman M and Winey K I 2006 *Macromolecules* **39** 5194
[3] Gupta S J, Prabhu P, Singh A, Sreeram B, Dhulia V, Yadav B S and Kanwar A 2009 *J. Mol. Cryst. Liquid Cryst.* **511** 1545
[4] Deshpande V D and Jape S 2009 *J. Appl. Polym. Sci.* **111** 1318
[5] Murthy N S, Zero K and Minor H 1994 *Macromolecules* **27** 1484
[6] Lin S B and Koenig J L 1982 *J. Polym. Sci.: Polym. Phys. Ed.* **20** 2277
[7] Lin S B and Koenig J L 1984 *J. Polym. Sci.: Polym. Symp.* **71** 121
[8] Oromiehie A and Mamizadeh A 2004 *Polym. Int.* **53** 728
[9] Hu G, Feng X, Zhang S and Yang M 2008 *J. Appl. Polym. Sci.* **108** 4080

[10] Hsiao A-E, Tsai S-Y, Hsu M-W and Chang S-J 2012 *Nanoscale Res. Lett.* **7** 240

[11] Mallakpour S and Zadehnazari A 2014 *Bull. Mater. Sci.* **37** 1065

[12] Song J, Liang J, Liu X, Krause W E, Hinestroza J P and Rojas O J 2009 *Thin Solid Films* **517** 4348

[13] Mazinani S, Ajji A and Dubois C 2010 *J. Polym. Sci.: Part B: Polym. Phys.* **48** 2052

[14] Xianwen R, Weng L T, Chan C-M and Ng K-M 2013 *Surf. Interface Anal.* **45** 1291

[15] Vedula J and Tonelli A E 2006 *J. Polym. Sci.: Part B* **45** 735

[16] Singh A R and Deshpande V D 2013 *AIP Conf. Proc.* **1538** 190

[17] Ubale A U, Sakhare Y S, Bhute M V, Belkhedkar M R and Singh A 2013 *Solid State Sci.* **16** 134e142

[18] Schmidt R H, Kinloch I A, Burgess A N and Windle A H 2007 *Langmuir* **23** 5707

[19] Prasad S G, De A and De U 2011 *Int. J. Spectrosc.* **2011** Article ID 810936

[20] Cole K C, Guevremont J, Ajji A and Dumoulin M M 1994 *Appl. Spectrosc.* **48** 1513

[21] Bullions T A, Wei M, Porbeni F E, Gerber M J, Peet J, Balik M, White J L and Tonelli A 2002 *J. Polym. Sci.: Part B: Polym. Phys.* **40** 992

[22] Ilišković N and Bravar M 1986 *Polym. Degrad. Stabil.* **15** 173

[23] Renyuan Q, Deyan S and Fuge Sun 1996 *Macromol. Chem. Phys.* **197** 1485

[24] Dhall S and Jaggi N 2014 *Bull. Mater. Sci.* **37** 1427

[25] Barbadikar D, Gautam R, Sahare S, Patrikar R and Bhatt J 2013 *Bull. Mater. Sci.* **36** 483

[26] Santhilkumar N, Sahoo N K, Thakur S and Tokas R B 2005 *Appl. Surf. Sci.* **252** 1608

[27] Manvi G, Singh A, Jagtap R N and Kothari D C 2012 *Prog. Org. Coat.* **75** 139

[28] Ferreira Q, Bernardo G, Charas A, Alcácer L and Morgado J 2010 *J. Phys. Chem. C* **114** 572

[29] Xu Y, Jia H-B, Piao J-N, Ye S-R and Huang J 2008 *J. Mater. Sci.* **43** 417